Received July 5, 2019, accepted July 22, 2019, date of publication July 29, 2019, date of current version August 14, 2019.

Digital Object Identifier 10.1109/ACCESS.2019.2931591

Novel Integrated Three-Port Bidirectional DC/DC Converter for Energy Storage System

YU-EN WU, (Member, IEEE), AND I-CHUN CHEN
Department of Electronic Engineering, National Kaohsiung University of Science and Technology, Kaohsiung, Taiwan
Corresponding author: Yu-En Wu (yew@nkfust.edu.tw)

ABSTRACT The study proposes a novel integrated three-port bidirectional dc/dc converter for energy storage systems. The converter includes two batteries, namely 24- and 48-V batteries, used as input source and for backup energy, respectively. Each battery can supply to dc load in the normal case. When the grid power fails, 24-V battery input is stepped up to the dc bus through a high step-up converter. The 48-V battery serves as a buffer power supply when the load increases instantaneously. At night, when the 48-V battery is under low power consumption, the dc bus can charge the battery. In addition, the converter can monitor both battery voltages simultaneously; when one battery is used excessively, the other battery can charge it, thus keeping the system power stable. The integrated three-port bidirectional dc/dc converter is a combination of a boost–flyback, forward converter, and voltage doubler and has the following advantages: 1) it operates in input continuous current and low voltage stress; 2) it provides input current recovery; 3) it improves high reverse voltage caused by the transformer; 4) it operates in zero current switching (ZCS); and 5) its doubler circuit can flexibly adjust the dc bus voltage. A 500-W three-port bidirectional dc/dc device was implemented to verify the feasibility and practicability of the proposed converter. The highest efficiency achieved for operation in 24-V battery high step-up mode was 95.3%; it was 94.9% and 95.2% in 48-V battery step-up and step-down mode, respectively.

INDEX TERMS Flyback converter, three-port bidirectional dc/dc converter, coupled inductor.

I. INTRODUCTION

Renewable energy is environment friendly and emits low pollution, but it has a disadvantage of unstable output DC voltage. For example, maximum solar energy can be obtained at noon but the output voltage and energy depend on the time and angle of the sun. While providing wind power to a generator, a fixed wind speed cannot be maintained and the output voltage is insufficient for direct supply to an inverter for conversion into AC voltage or supply load.

Nowadays, DC electronic products use batteries of different specifications. This study aims to step up a DC bus by providing 24-V and 48-V batteries to supply the DC load [1]–[9]. The 24-V battery is used as the auxiliary supply when the main power supply fails, whereas the 48-V battery supplies power under rapidly changing load. When the night power demand is low, the DC bus charges the battery. In addition, the two batteries can balance the energy by charging and discharging each other, thus maintaining a fixed amount of energy to the DC load. In addition, to prevent power failure at the main supply, the battery terminal can maintain a stable voltage to the DC bus and DC load (Fig. 1).

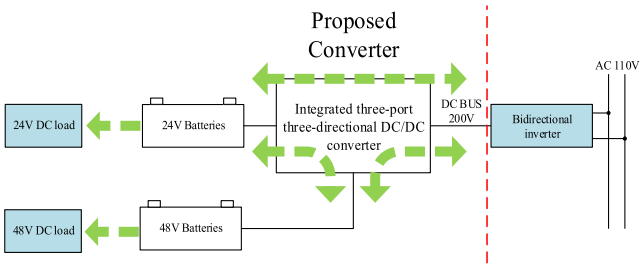

FIGURE 1. Proposed power system.

II. LITERATURE REVIEW

To reduce the number of components, cost, and volume of the converter, shared switches are used such that a bidirectional step-up/step-down converter can be realized. To add an energy storage battery to the regenerative energy system, a three-port-type circuit is used. Commonly used nonisolated

The associate editor coordinating the review of this manuscript and approving it for publication was Madhav Manjrekar.

three-port bidirectional DC/DC converters include high voltage gain boost-buck three-port bidirectional conversion circuits [18], and three-port bidirectional single-storage inductor DC/DC conversion circuits [19]. These nonisolated bidirectional DC/DC converters are low cost and have few components and simple control design. However, because of the fewer energy storage components, voltage gain increase in the circuit is difficult to achieve. Moreover, in the case of high power, the circuit becomes easily unstable, resulting in low efficiency, and because an isolation circuit is not used, the application of the converter is limited and the circuit is susceptible to interference. Isolated three-port bidirectional DC/DC converters include high-conversion-ratio half-bridge LLC bidirectional conversion circuits [17], three-port interleaved full-bridge conversion circuits [20], three-port half-bridge LLC resonant circuits [23], and high-voltage gain-doubler bidirectional circuits [24]. Half- and full-bridge architecture conversion circuits can realize the switching soft-cut function by using a phase shift control and the bidirectional function for efficiency by using a bypass diode. The use of LLC resonant circuits in the transformer design reduces the transformer volume and provides a wide range of voltage input; however, the design is difficult to implement and easily becomes unstable under light load, thereby lowering its efficiency. The control signal is interleaved to improve energy shortage and reduce the output inductor ripple. In recent years, many improved three-port bidirectional DC/DC converters, such as high-conversion-ratio half-bridge LLC bidirectional conversion circuits [17] with an interleaved forward circuit to recover leakage inductance energy and synchronous rectification to improve its efficiency, have been proposed, but the transformer in this converter is regarded as an ideal transformer, it is more impractical. Although the transformer has relatively few turns in the case of high power, the energy of the magnetizing inductor is released, affecting the efficiency. The three-port interleaved full-bridge conversion circuit [20] uses two inductors placed in an interleaved manner to charge the battery, and the secondary side uses the full bridge. In [21], [22], adjust the switch position so that the current flows through the bypass diode to simplify the circuit. A three-port half-bridge LLC resonant circuit [23] changes the secondary-side full-wave forward direction to two outputs, and the second-port voltage increasing circuit supplies energy to the third port. To increase the voltage gain, the solar input is connected in series with the boost circuit in front of the resonant circuit. To reduce the number of switches, the transformer winding is increased and used as a switch. However, the problems of poor response of the LLC under light load and low efficiency cannot be solved. Finally, a high-voltage-gain double-voltage bidirectional circuit [24] uses a voltage doubler circuit to realize a high step-up/step-down bidirectional circuit. In this converter, a set of three windings in the transformer, which reduces the number of inductors and transformers required. However, the primary side is subjected to excessive voltage stress, and the efficiency gradually decreases after reaching the maximum value under very light load.

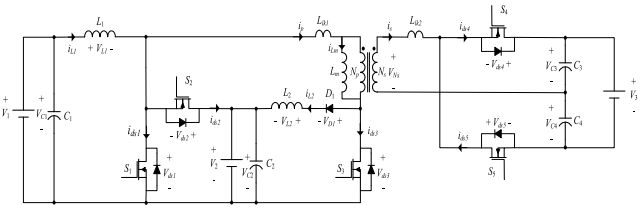

FIGURE 2. Integrated three-port bidirectional DC/DC converter.

III. PROPOSED CONVERTER AND OPERATIONAL PRINCIPLES

The integrated three-port bidirectional DC/DC converter combines a boost-flyback, forward converter and a voltage doubler. By using a common power switch and a diode to achieve a set of power supplies, power can be simultaneously supplied to the remaining two sets of the bidirectional output circuits [10]–[18], and the advantages of continuous input current of the booster circuit and high step-up are maintained. In addition, it can improve the problem that the larger instantaneous reverse voltage caused by the larger turns ratio of the transformer, as shown in Fig. 2. The V1, V2 and V3 voltages in the circuit are 24V, 48V and 200V respectively. The circuit architecture includes two energy storage inductors L1 and L2, a set of magnetizing inductor Lm, five power switches S1-5, a diode D1, and capacitors C1-4. The characteristic of the circuit is that the second power source is used as a relay capacitor, which can absorb the high reverse voltage and energy generated by the magnetizing inductance. When the power switches are switched each other, resonance can be generated by parasitic capacitance and leakage inductance on the switch to achieve secondary-side zero current switching (ZCS), improving the converter conversion efficiency and voltage gain.

The five switches of the integrated three-port bidirectional DC/DC converter circuit operate in the continuous conduction mode. First, a steady-state analysis of the circuit is performed by assuming the following conditions for simplicity:

(1) Both the power switches and the diode are assumed to be ideal components and the leakage inductance of the transformer is ignored.

(2) The equivalent magnetizing inductance Lm of the coupled inductor is considered.

(3) The capacitance of capacitors C1-4 is considered large enough to maintain voltages V_{C1-C4}.

A. 24-V VOLTAGE SOURCE

The circuit operation at 24-V input voltage can be divided into four modes. S1 and S5 and S2-4 operate in a mutually switching manner, where S1 and S5 are the main switches. The equivalent circuit and key waveforms of the operation mode are shown in Figs. 3 and 4.

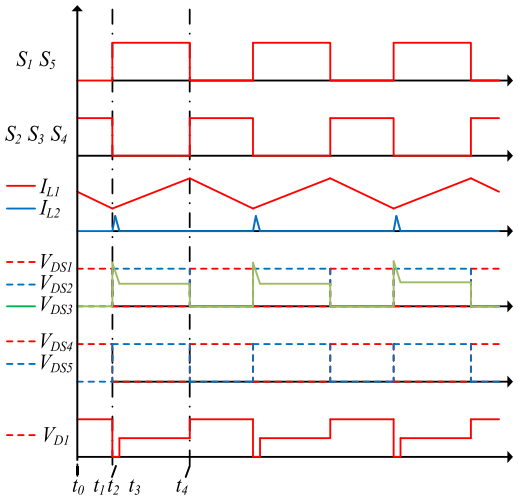

FIGURE 3. 24-V voltage source power switch operation situation.

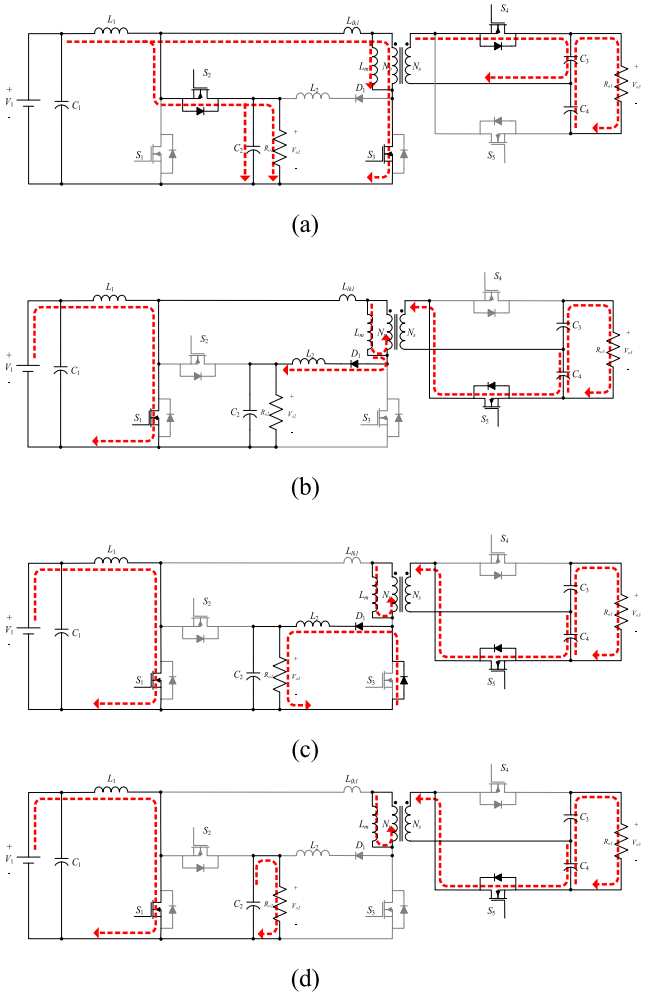

FIGURE 4. Integrated three-port bidirectional DC/DC converter circuit operating at 24-V input voltage in modes (a) 1, (b) 2, (c) 3, and (d) 4.

1) MODE 1 (FIG. 4(A), T0–T1)

Power switches S1 and S5 are turned off for a half cycle, whereas S2-4 are turned on. In this mode, the input voltage simultaneously outputs the energy on inductor L1 to load R_{o2} and stores energy to transformer magnetizing inductance Lm; inductor current i_{L1} linearly decreases to provide energy. At this time, energy ip stored in the magnetizing inductance is transmitted to the secondary side in the forward direction, such that the secondary side generates voltage V_{Ns}, stored in C3 through switch S4; finally, the energy in C3 and C4 is simultaneously supplied to load R_{o3}.

2) MODE 2 (FIG. 4(B), T1–T2)

When power switches S1 and S5 are turned on in a positive half cycle, S2-4 are turned off. In this mode, the input voltage crosses inductor L1 and inductor current i_{L1} increases linearly. At this time, the magnetizing inductance releases energy ip, which is reversely transmitted to the secondary side. A high voltage is instantaneously generated at switch S3, which drives D1 to conduct; the energy generated by the surge is absorbed back to capacitor C2. When the primary side of the transformer senses the current, the secondary side generates a voltage V_{NS}, stored in C4 through S5. Finally, the energy in C3 and C4 is simultaneously supplied to load Ro3.

3) MODE 3 (FIG. 4(C), T2–T3)

Power switches S1 and S5 are turned on for a positive half cycle, whereas S2-4 are turned off. D1 conducts the high voltage energy on the magnetizing inductor. When the surge voltage at the switch S3 is less than Vo2, the magnetizing inductor current is supplied only to the secondary terminal, and the energy stored in inductor L2 is bypassed by S3. The diodes release energy. At this time, the input power source continues to store energy in inductor L1, and the excitation inductor reverse energy generates secondary-side voltage V_{Ns}, which is stored in C4.

4) MODE 4 (FIG. (D), T3–T4)

Power switches S1 and S5 are turned on for a positive half cycle, whereas S2-4 are turned off, the energy of the inductor L2 is completely released and D1 is turned off. The excitation inductance simply outputs energy to the secondary side, which is released until the next cycle begins.

B. 48-V VOLTAGE SOURCE

The circuit operation at 48 V can be divided into three modes. S1 and S5 and S2-4 operate in a mutually switching manner, where S1 and S5 are the main switches. The equivalent circuit and key waveforms of the operation mode are as shown in Figs.5 and 6.

1) MODE 1 (FIG. 6(A), T0–T1)

Power switches S1 and S5 are turned on for a positive half cycle, whereas S2-4 are turned off. In this mode, the energy on inductor L1 is supplied to load Ro1 and inductor current i_{L1} linearly decreases to provide energy. In addition, when switch S3 instantaneously cuts off the surge voltage, the energy is absorbed by D1 and inductor L2. At this time,

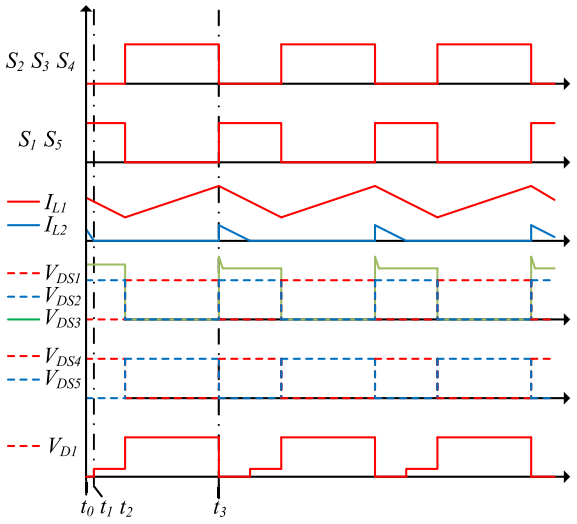

FIGURE 5. 48-V voltage source power switch operation situation.

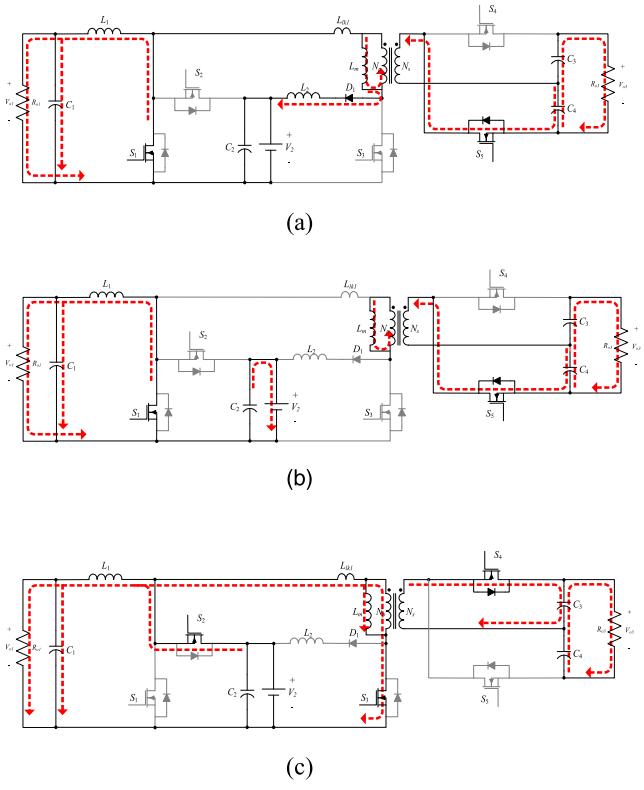

FIGURE 6. Integrated three-port bidirectional DC/DC converter circuit operating at 48-V input voltage in modes (a) 1, (b) 2, and (c) 3.

the magnetizing inductance releases the energy, which is reversely transmitted to the secondary side simultaneously; the secondary side generates voltage V_{Ns}, which is stored in C4 through switch S5. Finally, the energy in at C3 and C4 is simultaneously supplied to load R_{o3}.

2) MODE 2 (FIG. 6(B), T1–T2)

Power switches S1 and S5 are turned on for a positive half cycle, whereas S2-4 are turned off. Continuing from mode 1,

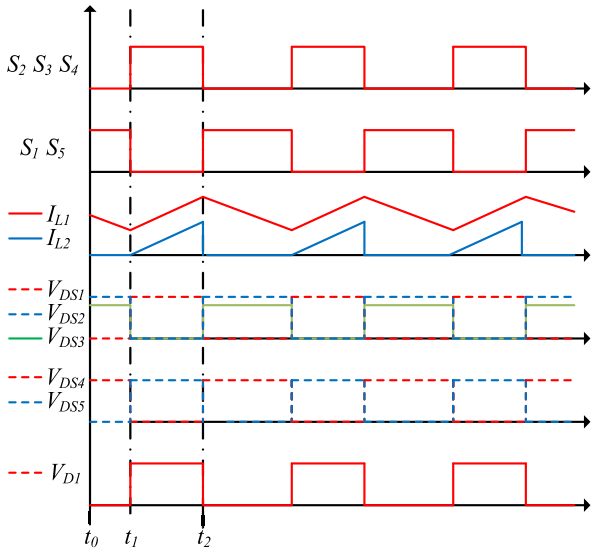

FIGURE 7. 200-V voltage source power switch operation situation.

after energy recovery on the magnetizing inductance, D1 is turned off, and the magnetizing inductance continuously outputs the remaining energy to the secondary side.

3) MODE 3 (FIG. 6(C), T2–T3)

Power switches S1 and S5 are turned off for a half cycle, whereas S2-4 are turned on. The input voltage stores energy to inductor L1, which is output to R_{o1}, and inductor current i_{L1} increases linearly. Simultaneously, the stored excitation energy ip is transmitted to the secondary side in the forward direction; the secondary side generates voltage V_{Ns}, which is stored in C3 through switch S4. Finally, the energy in C3 and C4 is simultaneously supplied to load R_{o3}. At the end of the state, power switches S1 and S5 are turned on and S2-4 are turned off instantaneously, causing a voltage surge at switch S3.

C. 200-V VOLTAGE SOURCE

The circuit operation at 200 V can be divided into two modes. S1 and S5 and S2-4 operate in a mutually switching manner, where S1 and S5 are the main switches. The equivalent circuit and key waveforms of the operation mode are as shown in Figs.7 and 8.

1) MODE 1 (FIG. 8(A), T0–T1)

Power switches S1 and S5 are turned on for a positive half cycle, while S2-4 are turned off. In this mode, the input voltage is divided into capacitors C3 and C4, and the energy stored in the magnetizing inductance Lm is absorbed back to the power supply terminal by switch S5 and simultaneously output to the secondary side load Ro2. Simultaneously, energy storage inductor L1 maintains the supply of energy to load R_{o1}, whereas current i_{L1} decreases linearly.

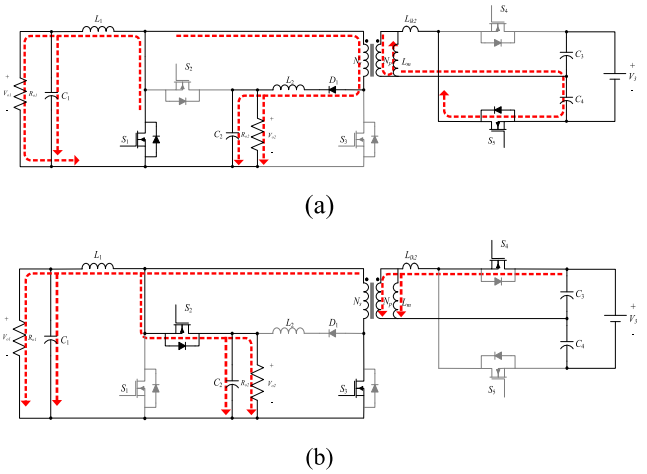

FIGURE 8. Integrated three-port bidirectional DC/DC converter circuit operating at 200-V input voltage in modes (a) 1 and (b) 2.

2) MODE 2 (FIG. 8(B), T1–T2)

Power switches S1 and S5 are turned off for a half cycle, whereas S2-4 are turned on. In this mode, the input voltage stores energy to the magnetizing inductor through switch S4 and outputs the energy to the secondary side in the forward direction. This generates voltage V_{Ns}, which supplies power to load R_{o2}. The energy is stored in inductor L1, and current i_{L1} increases linearly.

IV. STEADY-STATE ANALYSIS

A steady-state analysis of the integrated three-port bidirectional DC/DC converter circuit is conducted with its five switches operating in the continuous conduction mode. To simplify the analysis of the circuit, the following conditions are assumed:

(1) Both the power switches and the diode are assumed to be ideal components and the leakage inductance of the transformer is ignored.

(2) The equivalent magnetizing inductance Lm of the coupled inductor is considered.

(3) The capacitance of capacitors C1-4 is considered to be large enough to maintain voltages VC1–VC4.

A. 24-V BATTERY STEP-UP MODE

The on period of switches S1 and S5 is DTs, and the off period S2-4 is (1-D) Ts, as shown in Fig. 3. When switches S1, 5 are turned on and S2-4 are turned off, the amount of current change $\Delta\, i_{L1+}$ of inductor L_1 and the amount of current change $\Delta\, i_{Lm-}$ of the transformer can be obtained as follows:

$$\Delta i_{L1}^{+} = \frac{V_1}{L_1} \cdot D \cdot T_s \tag{1}$$

$$\Delta i_{Lm}^{-} = \frac{V_{C4} \cdot \frac{N_s}{N_p}}{L_m} \cdot (1-D) \cdot T_s \tag{2}$$

When switches S1 and S5 are turned off and S2-4 are turned on, the amount of current change $\Delta\, i_{L1+}$ of inductor L1 and the amount current change $\Delta\, i_{Lm-}$ of the transformer can be obtained as follows:

$$\Delta i_{L1}^{+} = \frac{V_{o2} - V_1}{L_1} \cdot (1-D) \cdot T_s \tag{3}$$

$$\Delta i_{Lm}^{-} = \frac{V_{o2}}{L_m} \cdot D \cdot T_s \tag{4}$$

By volt-second balance $\Delta\, i_{L1}^{+} = \Delta\, i_{Lm}^{-}$, the voltage gains Vo2 and Vo3 can be obtained as follows:

$$\frac{V_{o2}}{V_1} = \frac{1}{1-D} \tag{5}$$

$$\frac{V_{o3}}{V_1} = \frac{1}{1-D} \cdot \frac{N_s}{N_p}\left(1 + \frac{D}{1-D}\right) \tag{6}$$

B. 48-V BATTERY STEP-UP /STEP-DOWN MODE

The on period of switches S1 and S5 is DTs, and the off period of S2-4 is (1-D) Ts, as shown in Fig. 5. When switches S1 and S5 are turned on and S2-4 are turned off, the amount of current change Δi_{L1-} of inductor L_1 and the amount of current change Δi_{Lm-} of the transformer can be obtained as follows:

$$\Delta i_{L1}^{-} = \frac{V_{o1}}{L_1} \cdot (1-D) \cdot T_s \tag{7}$$

$$\Delta i_{Lm}^{-} = \frac{V_{C4} \cdot \frac{N_s}{N_p}}{L_m} \cdot (1-D) \cdot T_s \tag{8}$$

When switches S1 and S5 are turned off and S2-4 are turned on, the amount of current change Δi_{L1+} of inductor L1 and the amount of current change Δi_{Lm+} of the transformer can be obtained as follows:

$$\Delta i_{L1}^{+} = \frac{V_2 - V_{o1}}{L_1} \cdot D \cdot T_s \tag{9}$$

$$\Delta i_{Lm}^{+} = \frac{V_2}{L_m} \cdot D \cdot T_s \tag{10}$$

By volt-second balance $\Delta i_{L+} = \Delta i_{L-}$, the voltage gains V_{o1} and V_{o3} can be obtained as follows:

$$\frac{V_{o1}}{V_2} = D \tag{11}$$

$$\frac{V_{o3}}{V_2} = \frac{N_s}{N_p}\left(1 + \frac{D}{1-D}\right) \tag{12}$$

C. 200-V DC BUS STEP-DOWN MODE

The on period of switches S1 and S5 is DTs, and the off period of S2-4 is (1-D) Ts, as shown in Fig. 7.When switches S1 and S5 are turned on and S2-4 are turned off, the amount of current change Δi_{L1-} of inductor L_1 and the amount of current change Δi_{Lm-} of the transformer can be obtained as follows:

$$\Delta i_{L1}^{-} = \frac{V_{o1}}{L_1} \cdot (1-D) \cdot T_s \tag{13}$$

$$\Delta i_{Lm}^{-} = \frac{(V_{o2} \cdot \frac{N_p}{N_s})}{L_m} \cdot (1-D) \cdot T_s \tag{14}$$

When switches S1 and S5 are turned off and S2-4 are turned on, the amount of current change Δi_{L1+} of inductor L1 and

the amount of current change Δi_{Lm+} of the transformer can be obtained as follows:

$$\Delta i_{L1}^{+} = \frac{\left(\frac{V_3}{2} \cdot \frac{N_s}{N_p}\right) - V_{o1}}{L_1} \cdot D \cdot T_s \tag{15}$$

$$\Delta i_{Lm}^{+} = \frac{1}{2}\frac{V_3}{L_m} \cdot D \cdot T_s \tag{16}$$

By volt-second balance $\Delta i_{L+} = \Delta i_{L-}$, the voltage gains V_{o1} and V_{o2} can be obtained as follows:

$$\frac{V_{o1}}{V_3} = \frac{1}{2}\frac{N_s}{N_p}D \tag{17}$$

$$\frac{V_{o2}}{V_3} = \frac{1}{2} \cdot \frac{N_s}{N_p} \cdot \frac{D}{1-D} \tag{18}$$

V. DESIGN AND EXPERIMENTAL RESULTS

In this study, we implement an integrated three-port bidirectional converter with 500-W full load and 250-W power at each output and measure the power switches VGS, VDS, and I_{L1}; coupled inductor currents i_p and i_s; and important waveforms in each mode to verify the practicality of the converter. A microcontroller DSPIC30f4011 was employed as the basis of system control. Through digitized control, the problems of an overly complex hardware circuit and difficulty in designing the control circuit caused by the massive use of analog circuits can be avoided. With the control of MCU, the system can achieve the overcurrent and overvoltage protection. The electrical specifications of the system are shown in Table 1.

TABLE 1. The electrical specifications of the system.

Components	Parameters
Voltage of Batteries V_1	24V
Voltage of Batteries V_2	48V
Voltage of DC Bus V_3	200V
Switching frequency f	50kHz
Maximum output power P_o	500W
Capacitor C_1 and C_2	82uF/100V
Capacitor $C_{3\cdot4}$	100uF/400V
Power Switch $S_{1\sim5}$	IRFP4332
Diode D_1	MBR20200
Inductor $L_{1\cdot2}$	120uH
Magnetizing inductance L_m	183.4uH
Leakage inductance L_{lk1}	1.43uH
Turns ratio of transformer	1:2.1

In the 24-V set-up mode light load, input voltage V1 = 24 V, as shown in Fig. 9.

Fig. 9(a) and 9(b) shows switch control signals Vgs1, 2, storage inductor L1 current IL1, and switch voltage stress Vds1, 2. When switch S1 is turned on, energy is stored in inductor L_1, and after S1 is turned off, S2 is turned on and the inductor releases energy.

Fig. 9(c) and 9(d) shows switching signals Vgs1,3, transformer primary-side current ip, and switching voltage stress Vds1, 3. Switch S3 is turned on to store energy for the transformer, and the resonance is generated by the parasitic capacitance on the switch to achieve ZCS. Moreover, the reverse voltage on switch S3 is recovered at the off time.

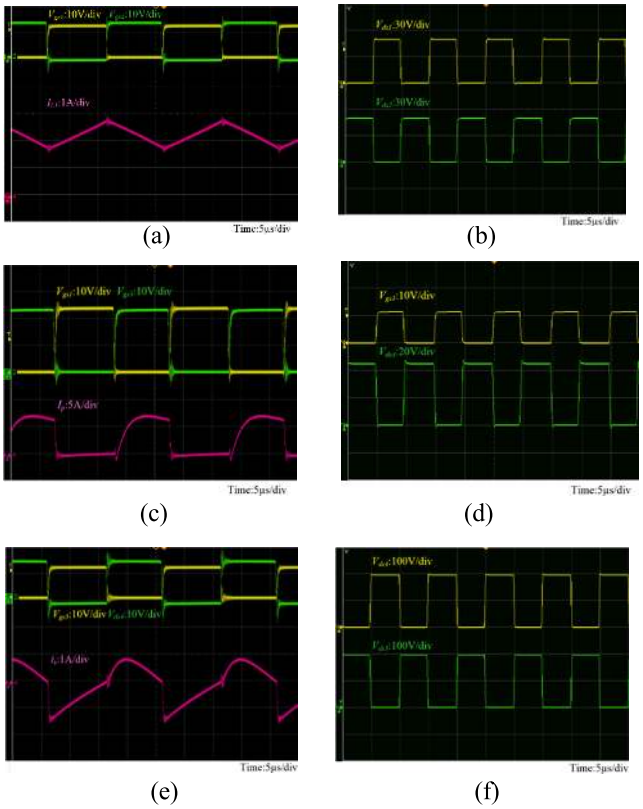

FIGURE 9. 24-V set-up mode light-loaded measured waveforms, (a) $V_{gs1,2}$ signals and inductor L_1 current waveform, (b) $V_{ds1,2}$ waveform, (c) $V_{gs1,3}$ signals and i_p waveform, (d) $V_{ds1,3}$ waveform, (e) $V_{gs4,5}$ signals and i_s waveform, and (f) $V_{ds4,5}$ waveform.

Fig. 9(e) and 9(f) shows switching signals Vgs4,5, transformer secondary-side current is, and switching voltage stress Vds4, 5. After amplifying the current generated on the primary side to the secondary side, the current can be reduced to zero by turning off the switch to achieve ZCS.

In the 24-V set-up mode half load, input voltage V_1 = 24 V, as shown in Fig. 10.

Fig. 10(a) and 10(b) shows switch control signals $V_{gs1,2}$, storage inductor L_1 current I_{L1}, and switch voltage stress $V_{ds1,2}$. After the load is aggravated, the current DC level rises because of the continuous current conduction mode (CCM).

Fig. 10(c) and 10(d) show switching signals $V_{gs1,3}$, transformer primary-side current ip, and switching voltage stress $V_{ds1,3}$. Compared with the light load current, it gradually stabilizes after entering the CCM, and the reverse voltage caused by the switch is not excessively generated.

Fig. 10(e) and 10(f) show switching signals $V_{gs4,5}$, transformer secondary-side current is, and switching voltage stress $V_{ds4,5}$. As the load changes, the current in the negative half cycle of the current can be stored again in capacitor C3 by turning on switch S4.

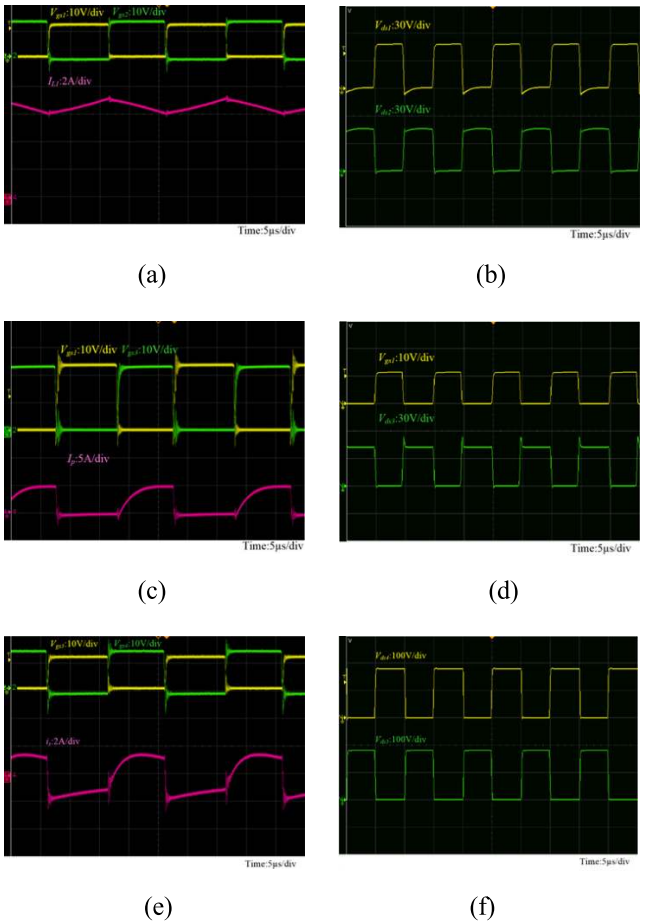

FIGURE 10. 24-V set-up mode half-load measured waveforms, (a) $V_{gs1,2}$ signals and inductor L_1 current waveform, (b) $V_{ds1,2}$ waveform, (c) $V_{gs1,3}$ signals and i_p waveform, (d) $V_{ds1,3}$ waveform, (e) $V_{gs4,5}$ signals and i_s waveform, and (f) $V_{ds4,5}$ waveform.

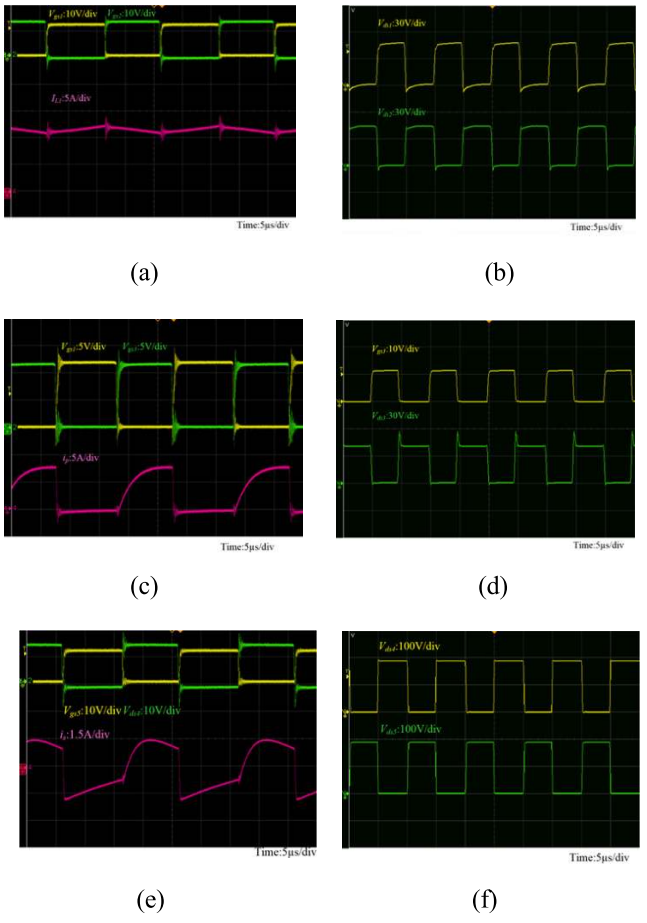

FIGURE 11. 24-V set-up mode full-load measured waveforms, (a) $V_{gs1,2}$ signals and inductor L_1 current waveform, (b) $V_{ds1,2}$ waveform, (c) $V_{gs1,3}$ signals and i_p waveform, (d) $V_{ds1,3}$ waveform, (e) $V_{gs4,5}$ signals and i_s waveform, and (f) $V_{ds4,5}$ waveform.

In the 24-V set-up mode full load, input voltage V1 = 24V, as shown in Fig. 11.

Fig. 11(a) and 11(b) shows switch control signals $V_{gs1,2}$, storage inductor L1 current I_{L1}, and switch voltage stress $V_{ds1,2}$. When the load is full, some micro-oscillation occurs when the switches are switched with each other, and the value of the stored energy inductor L1 is large, whereas the current ripple is small. When the switches S1 and S2 are switched to each other, as shown in Fig. 11(a), there is a short staggered period, which causes the inductor current to ring. It can be improved by setting the deadtime of the two switches or the signal up and down slope of the Gate-Source terminal of the switch.

Fig. 11(c) and 11(d) shows switching signals $V_{gs1,3}$, transformer primary-side current ip, and switching voltage stress $V_{ds1,3}$. After entering the full load, the current ip increases, and the reverse voltage of the main switch S3 increases slightly.

Fig. 11(e) and 11(f) show switching signals $V_{gs4,5}$, transformer secondary-side current is, and switching voltage stress $V_{ds4,5}$. The primary-side current of the transformer is amplified and output to the secondary side.

In the 48-V step-up/step-down mode light load, input voltage V2 = 48 V, as shown in Fig. 12.

Fig. 12(a) and 12(b) shows switch control signals Vgs1, 2, storage inductor L1 current I_{L1}, and switching voltage stress Vds1, 2. When switch S1 is turned on, the energy storage inductor L1 current releases energy to load Ro1, and switch S1 is turned off. When S2 is turned on, the power source stores energy to inductor L1, and the current increases linearly.

Fig. 12(c) shows switch control signals $V_{gs1,3}$, transformer primary-side current ip, and switching voltage stress V_{ds3}. When switch S3 is turned on, the power supply stores energy to the transformer and generates a current ip with the parasitic capacitance of the switch. The reverse voltage V_{ds3} and current change are checked when switch S3 is turned off.

Fig. 12(d) and 12(e) show switch control signals $V_{gs4,5}$, transformer secondary-side current is, and switching voltage stress $V_{ds4,5}$. After amplifying the current generated on the

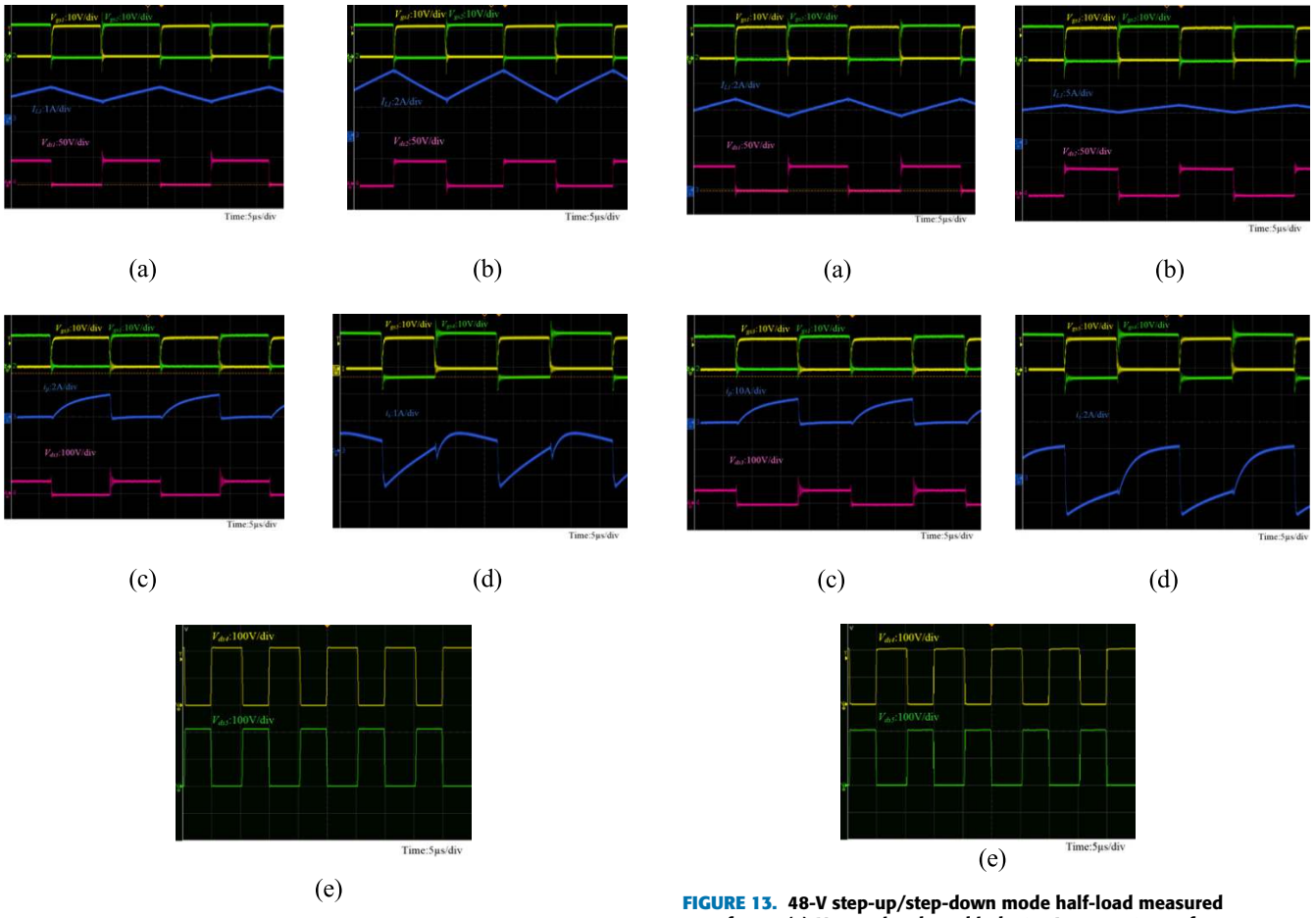

FIGURE 12. 48-V step-up/step-down mode light-load measured waveforms, (a) $V_{gs1,2}$ signals and inductor L_1 current waveform, (b) $V_{ds1,2}$ waveform, (c) $V_{gs1,3}$ signals and i_p waveform, (d) $V_{gs4,5}$ signals and i_s waveform, and (e) $V_{ds4,5}$ waveform.

FIGURE 13. 48-V step-up/step-down mode half-load measured waveforms, (a) $V_{gs1,2}$ signals and inductor L_1 current waveform, (b) $V_{ds1,2}$ waveform, (c) $V_{gs1,3}$ signals and i_p waveform, (d) V_{ds3} waveform, (e) $V_{gs4,5}$ signals and i_s waveform, and (f) $V_{ds4,5}$ waveform.

primary side to the secondary side, the current can be reduced to zero when the switch is turned off to achieve ZCS.

In the 48-V step-up/step-down mode half load, input voltage V2 = 48 V, as shown in Fig.13.

Fig. 13(a) and 13(b) shows switch control signals $V_{gs1,2}$, storage inductor L1 current I_{L1}, and switching voltage stress $V_{ds1,2}$. In the half load, the inductor L1 enters the CCM mode, and the DC level increases. Simultaneously, the surge voltage through the step-down circuit is not high.

Fig. 13(c) shows switch control signals $V_{gs1,3}$, transformer primary-side current ip, and switching voltage stress V_{ds3}. In the half load, when switch S3 is turned off, the resulting surge and light load do not considerably change, and the 48 V input source absorbs energy.

Figs. 13(d) and 13(e) shows switch control signals $V_{gs4,5}$, transformer secondary-side current is, and switching voltage stress $V_{ds4,5}$. When the switch S4 is turned on, the energy can be stored again in capacitor C3 in order to reduce the instantaneous change current when the switch is turned off.

In the 48-V step-up/step-down mode full load, input voltage V2 = 48 V, as shown in Fig. 14.

Fig. 14(a) and 14(b) shows switch control signals $V_{gs1,2}$, storage inductor L1 current I_{L1}, and switching voltage stress $V_{ds1,2}$. When the load is full load, the circuit is gradually stabilized, and the current increases steadily to the DC level. The design inductor L1 value is large, whereas the generated current ripple is small.

Fig. 14(c) shows switch control signals $V_{gs1,3}$, transformer primary-side current ip, and switching voltage stress V_{ds3}. When the load is full, the surge voltage and current ip increase slightly.

Fig. 14(d) and 14(e) show switch control signals $V_{gs4,5}$, transformer secondary-side current is, and switching voltage stress $V_{ds4,5}$. The primary-side current is amplified by the transformer and output to the secondary side. Compared with the current at half load, it is slightly affected by the switching and oscillates.

In the 200-V step-down mode light load, the circuit is changed to the reverse state, and the original secondary side is changed to the primary side, with input voltage V3 = 200 V, as shown in Fig.15.

Fig. 15(a) and 15(b) shows switch control signals $V_{gs4,5}$, transformer primary-side current ip, and switching voltage

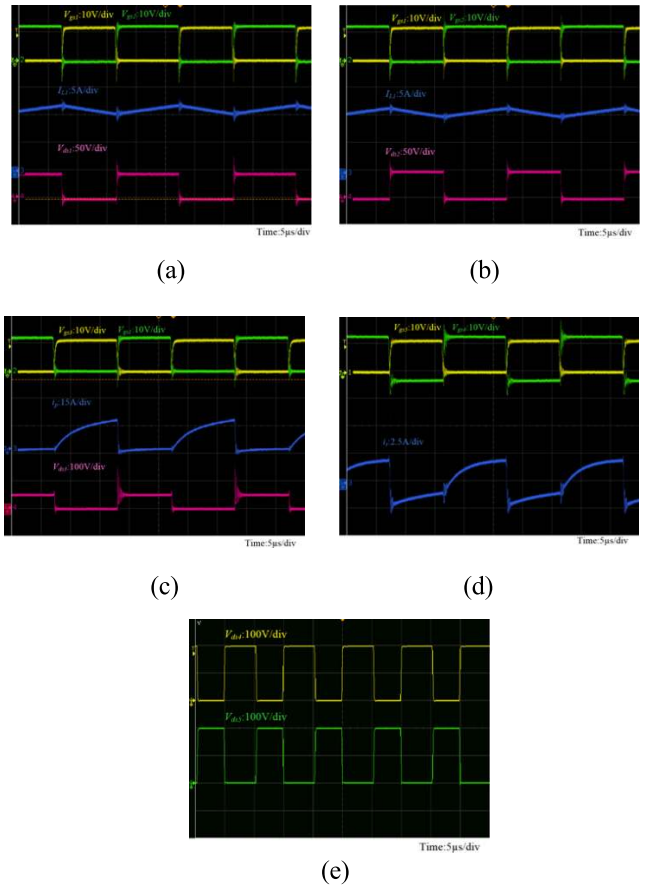

FIGURE 14. 48-V step-up/step-down mode full-load measured waveforms, (a) $V_{gs1,2}$ signals and inductor L_1 current waveform, (b) $V_{ds1,2}$ waveform, (c) $V_{gs1,3}$ signals and i_p waveform, (d) $V_{gs4,5}$ signals and i_s waveform, and (e) $V_{ds4,5}$ waveform.

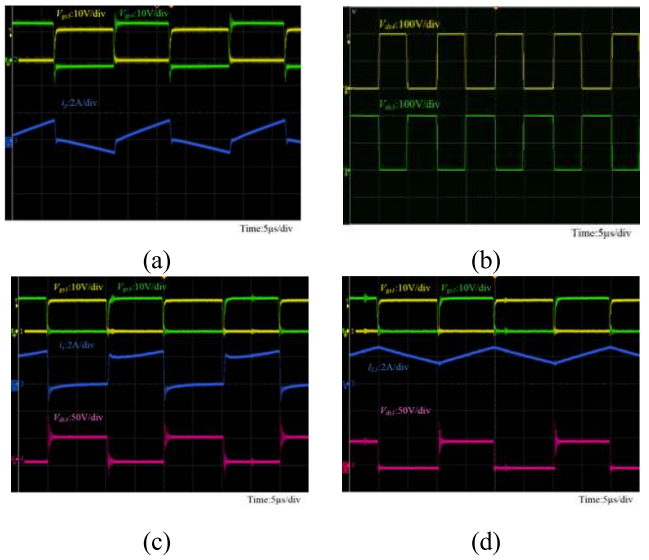

FIGURE 15. 200-V step-down mode light-load measured waveforms, (a) $V_{gs4,5}$ signals and i_p waveforms, (b) $V_{ds4,5}$ waveform, (c) $V_{gs1,3}$ signals and i_s waveforms, and (d) V_{ds1} and inductor L_1 current i_{L1} waveforms.

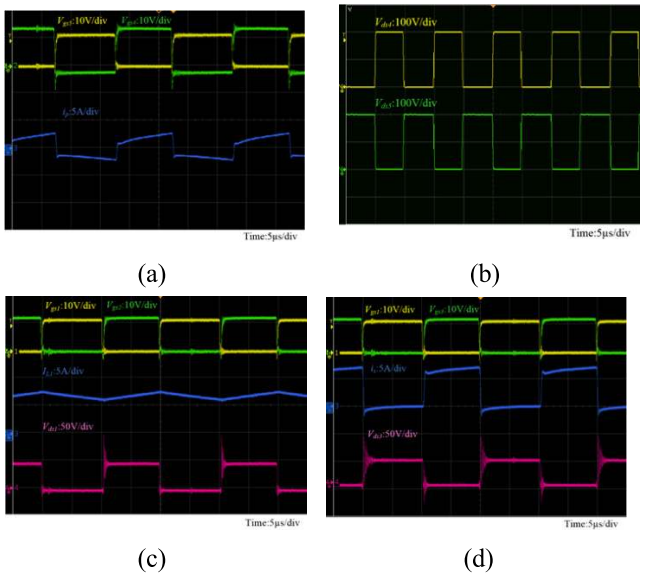

FIGURE 16. 200-V step-down mode half-load measured waveforms, (a) $V_{gs4,5}$ signals and i_p waveforms, (b) $V_{ds4,5}$ waveform, (c) $V_{gs1,3}$ signals and i_s waveforms, and (d) V_{ds1} and inductor L_1 current I_{L1} waveforms.

stress $V_{ds4,5}$. When switch S4 is turned on, power supply V3 stores energy to transformer Lm2, and when it turned off, switch S5 is turned on and the input current energy is recovered to the 200 V voltage source.

Fig. 15(c) shows switch control signals $V_{gs1,3}$, transformer secondary-side current is, and switching voltage stress Vds3. When switch S3 is turned on, the circuit serves as a forward circuit, and the primary-side current is supplied to Ro2 through the transformer. When switch S3 turned off, the reverse voltage of the transformer supplies energy to Ro2.

Fig. 15(d) shows switch control signals S1, 2, storage inductor L1 current IL1, and switching voltage stress V_{ds1}. When switch S1 is turned on, the circuit serves as a step-down circuit and the inductor L1 supplies energy to Ro1. When it is turned off, the transformer stores energy for L1. When the batteries deliver power, the ripple voltage appears at the DC bus is about 0.5%.

In the 200-V step-down mode half load, input voltage V3 = 200 V, as shown in Fig. 16.

Fig. 16(a) and 16(b) shows switch control signals $V_{gs4,5}$, transformer primary-side current ip, and switching voltage stress $V_{ds4,5}$. When switch S4 is turned on, the power supply V3 stores energy to the transformer Lm2; when it is turned off, switch S5 is turned on and the input current energy is recovered to the 200 V voltage source.

Fig. 16(c) shows switch control signals $V_{gs1,3}$, transformer secondary-side current is, and switching voltage stress Vds3. In the half load, the surge voltage increases slightly, and when switch S3 is turned off, the energy is absorbed back to the 48-V batteries through the D1 loop.

Fig. 16(d) shows switch control signals S1 and S2, storage inductor L1 current I_{L1}, and switching voltage stress V_{ds1}.

In the half load, the current DC level increases under the stable operation of the circuit.

In the 200-V step-down mode full load, input voltage V3 = 200 V, as shown in Fig.17.

Fig. 17(a) and 17(b) show switch control signals $V_{gs4,5}$, transformer primary-side current ip, and switching voltage stress $V_{ds4,5}$. When changing to the full load from the half load, current ip increases and the circuit remains stable.

Fig. 17(c) shows switch control signals $V_{gs1,3}$, transformer secondary-side current is, and switching voltage stress V_{ds3}. The voltage surge on switch S3 is close to that of the half load condition, and the energy is stably absorbed to the 48-V battery terminal.

Fig. 17(d) shows switch control signals S1 and S2, storage inductor L1 current I_{L1}, and switching voltage stress Vds1. When the switches are switched between each other, there will be some micro-oscillation during full load, but it will not affect the circuit action.

To prove the performance of the proposed converter, its characteristics are compared with other bidirectional converters to determine the advantages and disadvantages of the proposed architecture. Table 2 compares the components, their number, and the voltage gain of the proposed architecture with nonisolated architecture [19] and isolated architecture [20], [23], [24]. In the bidirectional architecture, many power switches and diodes are used. In the proposed architecture, the diode is replaced by a power switch as a bidirectional shared switch. Compared with others, the output and boost of the proposed architecture are higher and can be changed. The stage voltage doubler circuit is adjusted.

TABLE 2. Comparison of components and output numbers of various three-terminal bidirectional circuits.

literature / amount / Component and output	[19]	[20]	[23]	[24]	Proposed Converter
MOSFETs	4	6	3	4	5
diodes	5	2	3	0	1
capacitors	3	4	5	3	4
coupled inductor	0	1	1	2	1
inductors	1	2	2	0	2
input ports	2	2	2	2	3
output ports	2	2	2	2	3
voltage gain	$\frac{1}{(1-D)^2}$	$2\cdot\frac{N_s}{N_p}$	$(V_{in}+\frac{N_4}{N_3}\cdot V_{bat})\cdot(d_1+\Delta d_1)\cdot\frac{N_2}{N_1}$	$\frac{n}{1-2D_2}$	$\frac{1}{1-D}\cdot\frac{N_s}{N_p}(1+\frac{D}{1-D})$

Figs. 18–20 show the efficiency graphs of the proposed circuit. Figure 18 is a graph showing the efficiency of light load to full load measured by a 24-V battery as the input source. When the output power is 140 W, the maximum efficiency is 95.3%, and when the load is 250 W, the efficiency is 93.4%. Compared with [19], the proposed architecture shows higher output power performance. Although [20] and [23] have obvious differences in efficiency at light and half loads, however the circuit cannot be stabilized under full load. Compared with [24], the output power and efficiency are excellent at full load.

Fig. 19 shows the efficiency of light load to full load measured with the 48 V input source. When the output power

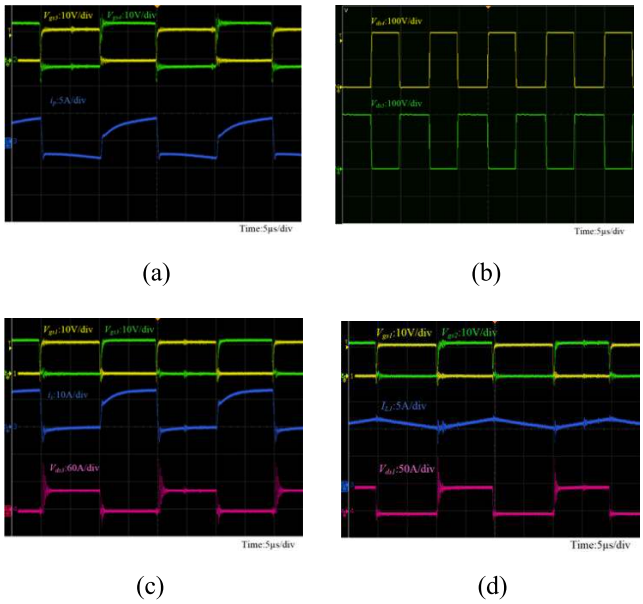

FIGURE 17. 200-V step-down mode full-load measured waveforms, (a) $V_{gs4,5}$ signals and i_p waveforms, (b) $V_{ds4,5}$ waveform, (c) $V_{gs1,3}$ signals and i_s waveforms, and (d) V_{ds1} and inductor L_1 current I_{L1} waveforms.

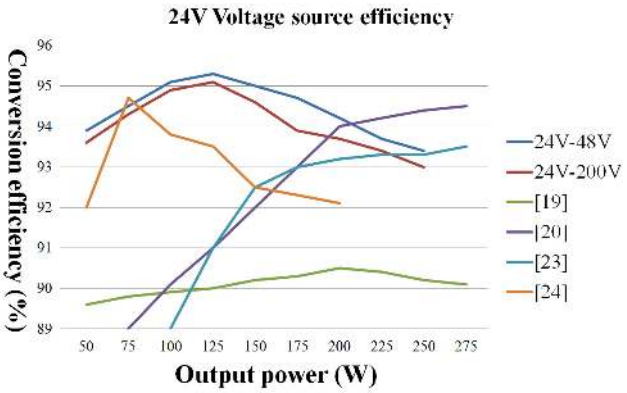

FIGURE 18. 24-V set-up mode efficiency curve.

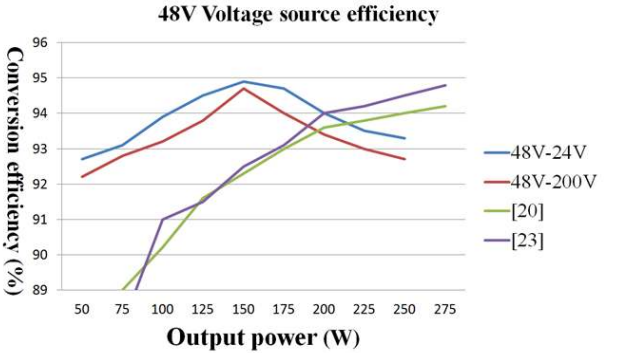

FIGURE 19. 48-V step-up/step-down mode efficiency curve.

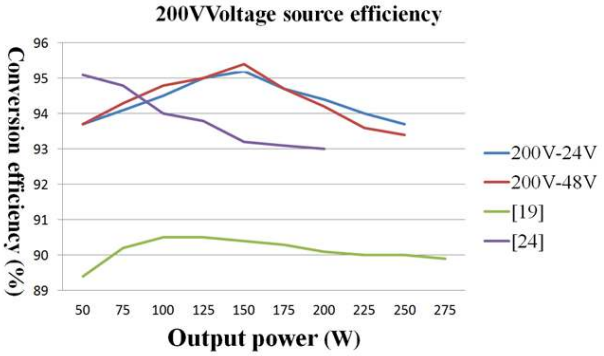

FIGURE 20. 200-V step-down mode efficiency curve.

is 150 W, the maximum efficiency is 94.9%, and when the full load is 250 W, the efficiency can reach 93.3%. The proposed architecture possesses higher efficiency than [20] and [23] at light load and half load.

Fig. 20 shows the efficiency of light load to full load measured with the 200 V input source. When the output power is 150 W, the maximum efficiency is 95.2%, and when the load is 250 W, the efficiency is 93.7%. Compared with [24], although the efficiency of the proposed architecture is slightly lower under light-load conditions, there are obvious excellent in output power and half and full load conditions.

VI. CONCLUSION

To eliminate the use of DC/DC converters of different specifications in electronic products, an integrated three-port bidirectional DC/DC converter circuit was proposed. This circuit uses a combination of the boost–flyback, forward converter, and voltage doubler of different specifications. The circuits are combined and the principle of switch sharing is used to achieve the effect of bidirectional mutual conduction. In addition, ZCS is achieved by using the leakage inductance of the transformer and the parasitic capacitance on the power switch to generate resonance. The second set of power supplies is used to absorb the high reverse voltage caused by the transformer, thereby improving the basic architecture, which would otherwise require the use of a high breakdown voltage switch. Thus, the overall output efficiency of the converter is increased. Finally, the circuit was implemented and tested to prove its feasibility. A double-ended 250-W circuit was realized. The step-up and step-down modes provided the maximum efficiencies of 95.3% and 95.2%, respectively.

REFERENCES

[1] L. Schmitz, R. F. Coelho, and D. C. Martins, "High step-up high efficiency DC-DC converter for module-integrated photovoltaic applications," in *Proc. IEEE 13th Brazilian Power Electron. Conf. 1st Southern Power Electron. Conf. (COBEP/SPEC)*, Fortaleza, Brazil, Nov./Dec. 2015, pp. 1–6.

[2] H.-W. Seong, H.-S. Kim, K.-B. Park, G.-W. Moon, and M.-J. Youn, "High step-up DC-DC converters using zero-voltage switching boost integration technique and light-load frequency modulation control," *IEEE Trans. Power Electron.*, vol. 27, no. 3, pp. 1383–1400, Mar. 2012.

[3] X. Ding, D. Yu, Y. Song, and B. Xue, "Integrated switched coupled-inductor boost-flyback converter," in *Proc. IEEE Energy Convers. Congr. Expo. (ECCE)*, Cincinnati, OH, USA, Oct. 2017, pp. 211–216.

[4] C.-H. Yeh, Y.-P. Hsieh, and J.-F. Chen, "A novel high step-up DC-DC converter with zero DC bias current coupled-inductor for microgrid system," in *Proc. 1st Int. Future Energy Electron. Conf. (IFEEC)*, Tainan, Taiwan, Nov. 2013, pp. 388–394.

[5] M. Muhammad, M. Armstrong, and M. A. Elgendy, "A nonisolated interleaved boost converter for high-voltage gain applications," *IEEE J. Emerg. Sel. Topics Power Electron.*, vol. 4, no. 2, pp. 352–362, Jun. 2016.

[6] Z. Liang, R. Guo, J. Li, and A. Q. Huang, "A high-efficiency PV module-integrated DC/DC converter for PV energy harvest in FREEDM systems," *IEEE Trans. Power Electron.*, vol. 26, no. 3, pp. 897–909, Mar. 2011.

[7] P. Wen, C. Hu, H. Yang, L. Zhang, C. Deng, Y. Li, and D. Xu, "A two stage DC/dc converter with wide input range for EV," in *Proc. Int. Power Electron. Conf. (IPEC-Hiroshima-ECCE ASIA)*, May 2014, pp. 782–789.

[8] A. I. Pressman, K. Billings, and T. Morey, *Switched Power Supply Design*, 3rd ed. Quanhua Book, 2012.

[9] H. M. Rashid, *Power Electronics: Circuits, Devices and Applications*, 3rd ed. Upper Saddle River, NJ, USA: Prentice-Hall, 2003, p. 712.

[10] H. W. R. Liang, J.-F. Chen, and C.-H. Lim, "Design and implementation of a bidirectional flyback boost/buck integrated converter," in *Proc. IEEE 2nd Annu. Southern Power Electron. Conf. (SPEC)*, Auckland, New Zealand, Dec. 2016, pp. 1–6.

[11] R. J. Wai and J. J. Liaw, "High-efficiency-isolated single-input multiple-output bidirectional converter," *IEEE Trans. Power Electron.*, vol. 30, no. 9, pp. 4914–4930, Sep. 2015.

[12] B. Zhang, P. Wang, T. Bei, X. Li, Y. Che, and G. Wang, "Novel topology and control of a non-isolated three port DC-DC converter for PV-battery power system," in *Proc. 20th Int. Conf. Elect. Mach. Syst. (ICEMS)*, Aug. 2017, pp. 1–6.

[13] R. Faraji and H. Farzanehfard, "Soft-switched nonisolated high step-up three-port DC–DC converter for hybrid energy systems," *IEEE Trans. Power Electron.*, vol. 33, no. 12, pp. 10101–10111, Dec. 2018.

[14] H. Zhu, D. Zhang, B. Zhang, and Z. Zhou, "A nonisolated three-port DC–DC converter and three-domain control method for PV-battery power systems," *IEEE Trans. Ind. Electron.*, vol. 62, no. 8, pp. 4937–4947, Aug. 2015.

[15] J. Zeng, W. Qiao, and L. Qu, "An isolated three-port bidirectional DC-DC converter for photovoltaic systems with energy storage," in *Proc. IEEE Ind. Appl. Soc. Annu. Meeting*, Lake Buena Vista, FL, USA, Oct. 2013, pp. 1–8.

[16] K. K. Gokul, B. P. Emmanuel, S. Ashok, and S. Kumaravel, "Design and control of non-isolated bidirectional DC-DC converter for energy storage application," in *Proc. 2nd IEEE Int. Conf. Recent Trends Electron., Inf. Commun. Technol. (RTEICT)*, May 2017, pp. 289–293.

[17] T.-J. Liang and J.-H. Lee, "Novel high-conversion-ratio high-efficiency isolated bidirectional DC–DC converter," *IEEE Trans. Ind. Electron.*, vol. 62, no. 7, pp. 4492–4503, Jul. 2015.

[18] L.-J. Chien, C.-C. Chen, J.-F. Chen, and Y.-P. Hsieh, "Novel three-port converter with high-voltage gain," *IEEE Trans. Power Electron.*, vol. 29, no. 9, pp. 4693–4703, Sep. 2014.

[19] T. Cheng, D. D.-C. Lu, and L. Qin, "Non-isolated single-inductor DC/DC converter with fully reconfigurable structure for renewable energy applications," *IEEE Trans. Circuits Syst. II, Exp. Briefs*, vol. 65, no. 3, pp. 351–355, Mar. 2018.

[20] H. Wu, J. Zhang, X. Qin, T. Mu, and Y. Xing, "Secondary-side-regulated soft-switching full-bridge three-port converter based on bridgeless boost rectifier and bidirectional converter for multiple energy interface," *IEEE Trans. Power Electron.*, vol. 31, no. 7, pp. 4847–4860, Jul. 2016.

[21] X. Sun, Y. Shen, W. Li, and H. Wu, "A PWM and PFM hybrid modulated three-port converter for a standalone PV/battery power system," *IEEE J. Emerg. Sel. Topics Power Electron.*, vol. 3, no. 4, pp. 984–1000, Dec. 2015.

[22] M. C. Mira, Z. Zhang, A. Knott, and M. A. E. Andersen, "Analysis, design, modeling, and control of an interleaved-boost full-bridge three-port converter for hybrid renewable energy systems," *IEEE Trans. Power Electron.*, vol. 32, no. 2, pp. 1138–1155, Feb. 2017.

[23] H. Zhu, D. Zhang, H. S. Athab, B. Wu, and Y. Gu, "PV isolated three-port converter and energy-balancing control method for PV-battery power supply applications," *IEEE Trans. Ind. Electron.*, vol. 62, no. 6, pp. 3595–3606, Jun. 2015.

[24] C.-L. Shen, S.-Y. Shen, P.-C. Chiu, and T.-C. Liang, "Isolated bidirectional converter with minimum active switches for high-voltage ratio achievement and micro-grid applications," *IET Power Electron.*, vol. 10, no. 15, pp. 2208–2216, Aug. 2017.

YU-EN WU was born in Chiayi, Taiwan, in 1964. He received the B.S. degree from the Taiwan Institute of Technology, Taipei, Taiwan, in 1989, the M.S. degree from Sun Yat-sen University, Kaohsiung, Taiwan, in 1992, and the Ph.D. degree from National Chung Cheng University, Chiayi, in 2005, all in electrical engineering.

From 1992 to 2005, he was a Lecturer with the Department of Electronic Engineering, Wu Feng Institute of Technology, Chiayi, where he was an Associate Professor. He is currently a Professor with the Department of Electronic Engineering, National Kaohsiung University of Science and Technology. His research interests include bidirectional dc/dc converter and implementation of multi-inverter systems, power electronics, DSP-based application systems, smart grid, and renewable energy systems.

I-CHUN CHEN was born in New Taipei City, Taiwan, in 1994. He received the B.S. degree in electronics engineering and the M.S. degree in electrical engineering from the Kaohsiung First University of Science and Technology, Kaohsiung, Taiwan, in 2016 and 2018, respectively. His research interests include renewable energy sources and energy management.